Numerical evaluation of coherent-state path integrals in quantum dynamics

1999 J. Phys. A: Math. Gen. 32 2075

(http://iopscience.iop.org/0305-4470/32/11/004)

J. Phys. A: Math. Gen. **32** (1999) 2075–2090. Printed in the UK PII: S0305-4470(99)98548-7

Numerical evaluation of coherent-state path integrals in quantum dynamics

B Burghardt and J Stolze

Institut für Physik, Universität Dortmund, 44221 Dortmund, Germany

Received 21 October 1998

Abstract. The numerical evaluation of coherent-state path integrals for quantum dynamical problems is discussed for one-dimensional examples. To propagate an initial state, we use the normal and antinormal ordered coherent-state path integrals combined with a split-operator technique dividing the Hamiltonian into harmonic and anharmonic parts. For numerical purposes integrations must be approximated by quadrature formulae. This leads to a matrix multiplication scheme which is systematically tested for the double-well and Morse potentials. The method is accurate for propagation times much longer than the natural time scale of the system, and it allows for short as well as long time steps without loss of stability.

1. Introduction

Ever since its invention 50 years ago, path integration has been an important tool of quantum physics. Most of the applications of path integration are based on the real-space path integral involving the Feynman–Kac formula for integration over paths $\vec{r}(t)$ in configuration space. Apart from the traditional path integration in configuration space there is the path integration using coherent states (Klauder and Skagerstam 1985, Perelomov 1986). Although the coherent-state path integral has made it into the textbook literature (Schulman 1981), it is only infrequently applied as a numerical tool (Adachi 1989, Marchioro 1990, Marchioro and Beck 1992, Caratzoulas and Pechukas 1996).

In a recent paper (Burghardt *et al* 1998) we have demonstrated that coherent-state path integration may be employed for the numerical evaluation of partition functions and other quantities in equilibrium statistical mechanics, for temperatures ranging from zero way up into the regime where quantum effects are negligible. Here we want to discuss real-time applications as opposed to the imaginary-time applications discussed in our previous paper; that is, we are dealing with the time evolution operator instead of the density operator. There exists a large variety of techniques† for propagating a given initial state under the influence of a given Hamiltonian. A very popular class of propagation algorithms are the so-called split-operator techniques (Feit *et al* 1982). These techniques are based on a decomposition of the time evolution operator into kinetic and potential parts which are most easily handled in the momentum and position representations, respectively. The necessary frequent switching between these two representations can be handled efficiently by fast Fourier transform methods. In this paper we want to introduce split-operator ideas into the numerical evaluation of coherent-state path integrals (CSPIs), by dividing the given Hamiltonian into harmonic and anharmonic

† See, for example, several contributions to *Comput. Phys. Commun.* **63** (1991), special issue on Time-Dependent Methods for Quantum Dynamics, or Kosloff (1994), Leforestier *et al* (1991).

0305-4470/99/112075+16$19.50

parts. Our method will then be able to exploit the trivial time evolution of a coherent state in a harmonic oscillator in the same way as the conventional split-operator techniques exploit the trivial free time evolution of a plane-wave state. In fact, a division of the Hamiltonian into harmonic and anharmonic parts has been suggested earlier (Mak and Andersen 1990, Prates Ramalho *et al* 1993) in the context of real-space path integration, but we think that the idea fits much more naturally into the context of coherent-state path integration. The reason for this belief is easily understood: in the context of real-space path integration the usual quantity to be studied is the matrix element of the propagator (or time evolution operator) between two position eigenstates. A position eigenstate contains components of arbitrarily high momentum which travel at arbitrarily high speed. Consequently the propagator matrix element does not decay as a function of distance, but it oscillates progressively faster at larger distances. This leads to the well known problems concerning integrals with rapidly oscillating integrands. This free-particle scenario does not change fundamentally in the presence of a potential†.

In contrast to a position eigenstate, a coherent state is a smooth minimum-uncertainty Gaussian wavepacket, which in a harmonic oscillator potential neither spreads nor picks up rapidly varying phase factors. The time dependence of the harmonic propagator matrix element between coherent states consequently is completely trivial. This changes as anharmonicities are added, but not fundamentally, as we shall see by way of example below. The coherent state propagator matrix element thus is a complex function with smoothly decaying amplitude and slowly varying phase.

We consider the matrix element of the time evolution operator between given initial and final states. For numerical purposes the path integral representation of that quantity must be approximated by an N-dimensional integral (where N is often called the Trotter number). The integrand is a product of matrix elements of time evolution operators for individual short time intervals. One approximation of crucial importance in any numerical path integral scheme then is the approximate calculation of these short-time matrix elements, which we will achieve by splitting the Hamiltonian into a harmonic part, which can be treated exactly, and an anharmonic part. With this split-operator technique it is possible to use efficient high-order approximations for the anharmonic part of the integrand. The remaining important approximation is the numerical evaluation of the N integrations involved. If that is done via quadrature formulae with fixed abscissas, the path integration can be mapped to an iterated matrix multiplication‡. A possible alternative§ is the stochastic (Monte Carlo (MC)) evaluation of the multidimensional integral approximating the path integral. Apart from some remarks (section 6), however, we will not treat MC methods here but concentrate on the matrix multiplication approach.

An early numerical application of CSPIs to quantum dynamics is the paper by Adachi (1989), discussing the semiclassical CSPI for the kicked rotator.

In this paper we want to demonstrate that coherent-state path integration as outlined above is a useful numerical tool in quantum dynamics, and we discuss the influence of various technical parameters.

The plan of the paper is as follows. In section 2 we fix the notation for the CSPI. In section 3 we introduce the split-operator technique. In section 4 we describe a matrix multiplication scheme, which we use in section 5 to calculate CSPIs for some simple anharmonic systems, namely a particle in the double-well potential, and in the Morse potential. In this section we also discuss the influence of various technical parameters. Section 6 concludes the paper.

† We leave aside the special case of the harmonic oscillator where the propagator is a strictly periodic function of time and thus an arbitrary initial state refocuses periodically.

‡ See Burghardt *et al* (1998) and references therein: e.g. Storer (1968).

§ See Marchioro and Beck (1992) for an early application of MC methods to CSPIs.

2. Coherent-state path integrals

Throughout this paper, we will consider a standard Hamiltonian

$$H = T + V = \frac{P^2}{2m} + V(Q) \tag{1}$$

for a system with one degree of freedom, described by the momentum operator P and the position operator Q.

A coherent state $|\alpha\rangle$ may be defined by means of harmonic oscillator creation and annihilation operators $a^\dagger$ and a,

$$a := \frac{1}{\sqrt{2\hbar}}\left(\sqrt{m\omega}Q + \mathrm{i}\frac{1}{\sqrt{m\omega}}P\right) \tag{2}$$

through

$$|\alpha\rangle := \exp(\alpha a^\dagger - \alpha^* a)|0\rangle \tag{3}$$

where $|0\rangle$ is the normalized oscillator ground state, and the exponential is a displacement operator.

Two basic facts about coherent states are essential in our context. First, $|\alpha\rangle$ is an eigenstate of the annihilation operator,

$$a|\alpha\rangle = \alpha|\alpha\rangle \tag{4}$$

(note that the frequency ω, and hence the characteristic length scale $(\hbar/m\omega)^{-1/2}$, is completely arbitrary and can be used as an adjustable parameter). The second feature is the resolution of unity

$$\int \frac{\mathrm{d}^2\alpha}{\pi}|\alpha\rangle\langle\alpha| = \mathbb{1} \tag{5}$$

($\mathrm{d}^2\alpha := \mathrm{d}\,\mathrm{Re}\,\alpha\,\mathrm{d}\,\mathrm{Im}\,\alpha$).

It is also noteworthy that the coherent states are normalized, but not orthogonal

$$\langle\alpha|\alpha'\rangle = \exp\left(-\frac{|\alpha|^2}{2} - \frac{|\alpha'|^2}{2} + \alpha^*\alpha'\right). \tag{6}$$

The position space representation of a coherent state is given by

$$\langle x|\alpha\rangle = \pi^{-1/4}\exp[-\tfrac{1}{2}(x^2 + \alpha^2) + \sqrt{2}x\alpha - \tfrac{1}{2}|\alpha|^2]. \tag{7}$$

Before defining CSPIs, we introduce the normal and antinormal symbols of an operator A. The normal symbol $A_+(\alpha, \alpha')$ is defined by

$$A_+(\alpha, \alpha') := \frac{\langle\alpha|A|\alpha'\rangle}{\langle\alpha|\alpha'\rangle}. \tag{8}$$

An obvious way to evaluate it is by normal-ordering the operator A (i.e. writing A in terms of $a^\dagger$ and a so that in every term all $a^\dagger$ stand to the left of all a) and then (by equation (4)) replacing $a^\dagger$ by α^* and a by α'. The antinormal symbol $A_-(\alpha)$ is defined by

$$A = \int \frac{\mathrm{d}^2\alpha}{\pi}|\alpha\rangle\langle\alpha|A_-(\alpha) \tag{9}$$

and can be obtained by bringing A into antinormal form (a left of $a^\dagger$) and replacing a by α, $a^\dagger$ by α^*. Note that in contrast to A_+, A_- depends only on one complex argument. Whereas $A_+(\alpha, \alpha')$ exists for all practically relevant operators, $A_-(\alpha)$ is a much more delicate function and it exists only for a restricted class of operators.

We now can define the discretized CSPI representation for the matrix element of the propagator between coherent states in two different ways. We first define the normal CSPI (NCSPI) ($\alpha_0 \equiv \alpha, \alpha_{N+1} \equiv \alpha'$)

$$U(\alpha,\alpha';N) := \int \frac{\mathrm{d}^2\alpha_1}{\pi} \ldots \int \frac{\mathrm{d}^2\alpha_N}{\pi} \prod_{\nu=1}^{N+1} \langle \alpha_{\nu-1}|\alpha_\nu\rangle \prod_{\nu=1}^{N} \left(\exp\left(-\frac{\mathrm{i}t}{\hbar N}H\right)\right)_+ (\alpha_{\nu-1},\alpha_\nu). \quad (10)$$

Similarly, the antinormal CSPI (ACSPI) is defined as follows:

$$U(\alpha,\alpha';N) := \int \frac{\mathrm{d}^2\alpha_1}{\pi} \ldots \int \frac{\mathrm{d}^2\alpha_N}{\pi} \prod_{\nu=1}^{N+1} \langle \alpha_{\nu-1}|\alpha_\nu\rangle \prod_{\nu=1}^{N} \left(\exp\left(-\frac{\mathrm{i}t}{\hbar N}H\right)\right)_- (\alpha_\nu). \quad (11)$$

More general definitions of a CSPI are also known (Leschke 1979), but we restrict ourselves to the NCSPI and ACSPI defined above and therefore do not discuss the generalization here.

We conclude this general section by pointing out that the antinormal symbol of a Hermitian Hamiltonian H is a real-valued function.

3. Split-operator methods

In general, neither the normal symbol nor the antinormal symbol of the propagator $\exp(-\mathrm{i}tH/\hbar)$ can be found explicitly. Also, though it might be possible to calculate the series expansion of the propagator to any desired order by ordering powers of H, this way is for many Hamiltonians too tedious. Therefore we divide the Hamiltonian (equation (1)) into two parts: $H = H_0 + \tilde{V}(Q)$, where $H_0 = \hbar\omega(a^\dagger a + \frac{1}{2})$ is the Hamiltonian of the harmonic oscillator and $\tilde{V}(Q) = V(Q) - \frac{m\omega}{2\hbar}Q^2$, and apply the Zassenhaus formula

$$\exp\left[-\frac{\mathrm{i}}{\hbar}t(H_0+\tilde{V})\right] = \exp\left(-\frac{\mathrm{i}t}{2\hbar}H_0\right)\exp\left(-\frac{\mathrm{i}}{\hbar}t\tilde{V}\right)\exp\left(-\frac{\mathrm{i}t}{2\hbar}H_0\right) + \mathcal{O}(t^3). \quad (12)$$

In the context of configuration space path integration it would look more natural to decompose the Hamiltonian into a kinetic term T and a potential one $V(Q)$. That decomposition is well known in the field of wavepacket propagation and is called split-operator technique (Feit *et al* 1982). In our case the splitting of the Hamiltonian into a harmonic and an anharmonic part has the advantage that the harmonic time evolution of a coherent state is simple:

$$\exp\left(-\frac{\mathrm{i}}{\hbar}tH_0\right)|\alpha\rangle = \mathrm{e}^{-\mathrm{i}\omega t/2}|\mathrm{e}^{-\mathrm{i}\omega t}\alpha\rangle \quad (13)$$

that is a rotation of the state $|\alpha\rangle$ in the complex plane and multiplication by a phase factor.

Together with equation (10) (NCSPI) the propagation of a coherent state $|\alpha\rangle$ by a time step $\Delta t = t/N$ is given by

$$\begin{aligned}\mathrm{e}^{-\frac{\mathrm{i}}{\hbar}\frac{t}{N}H}|\alpha\rangle &\simeq \int \frac{\mathrm{d}^2\alpha'}{\pi}|\alpha'\rangle\langle\alpha'|\mathrm{e}^{-\frac{\mathrm{i}}{\hbar}\frac{t}{2N}H_0}\mathrm{e}^{-\frac{\mathrm{i}}{\hbar}\frac{t}{N}\tilde{V}}\mathrm{e}^{-\frac{\mathrm{i}}{\hbar}\frac{t}{2N}H_0}|\alpha\rangle \\ &= \mathrm{e}^{-\mathrm{i}\frac{\omega t}{2N}}\int \frac{\mathrm{d}^2\alpha'}{\pi}|\alpha'\rangle\left(\exp\left(-\frac{\mathrm{i}t}{\hbar N}\tilde{V}\right)\right)_+ (\alpha'\mathrm{e}^{+\mathrm{i}\frac{\omega t}{2N}},\alpha\mathrm{e}^{-\mathrm{i}\frac{\omega t}{2N}})\langle\alpha'\,\mathrm{e}^{+\mathrm{i}\frac{\omega t}{N}}|\alpha\rangle. \quad (14)\end{aligned}$$

The application to the ACSPI is slightly different:

$$\begin{aligned}\mathrm{e}^{-\frac{\mathrm{i}}{\hbar}\frac{t}{N}H}|\alpha\rangle &\simeq \mathrm{e}^{-\frac{\mathrm{i}}{\hbar}\frac{t}{2N}H_0}\left(\int \frac{\mathrm{d}^2\alpha'}{\pi}|\alpha'\rangle\langle\alpha'|\left(\exp\left(-\frac{\mathrm{i}t}{\hbar N}\tilde{V}\right)\right)_-(\alpha')\right)\mathrm{e}^{-\frac{\mathrm{i}}{\hbar}\frac{t}{2N}H_0}|\alpha\rangle \\ &= \mathrm{e}^{-\mathrm{i}\frac{\omega t}{2N}}\int \frac{\mathrm{d}^2\alpha'}{\pi}|\alpha'\rangle\left(\exp\left(-\frac{\mathrm{i}t}{\hbar N}\tilde{V}\right)\right)_-(\alpha'\mathrm{e}^{+\mathrm{i}\frac{\omega t}{2N}})\langle\alpha'\mathrm{e}^{+\mathrm{i}\frac{\omega t}{N}}|\alpha\rangle. \quad (15)\end{aligned}$$

The propagation of an arbitrary state $|\psi\rangle$ can be effected in an obvious way by recalling that due to the completeness of the coherent states $|\psi\rangle$ can be written

$$|\psi\rangle = \int \frac{\mathrm{d}^2\alpha}{\pi} |\alpha\rangle\langle\alpha|\psi\rangle. \tag{16}$$

In both cases the remaining problem is to evaluate the normal or antinormal symbol of $\exp(-\frac{\mathrm{i}t}{\hbar N}\tilde{V})$. As an approximation of this symbol we use the symbol of the series expansion of the exponential up to a certain order, assuming that the symbol of any power of $\tilde{V}$ is known. This is possible, for example, if $\tilde{V}$ is a polynomial in Q and $\exp(Q)$. In the figures and tables relating to the numerical examples to be discussed below we always state the order of the expansion.

At this point we would like to relate our work to important earlier papers (Marchioro 1990, Marchioro and Beck 1992) on CSPI. Whereas Marchioro (1990) contains a rather detailed discussion of the general properties of ACSPI and NCSPI, Marchioro and Beck (1992) suggest an approach similar to ours. The strategy suggested there is to write the Hamiltonian as $H = H_0 + V_\mathrm{I}$ with H_0 a quadratic form in coordinates and momenta, and V_I a function of the coordinates only. (This is similar to our approach, but we suggest always using the harmonic oscillator for H_0, because the corresponding coherent-state matrix elements are known analytically and their numerical evaluation is trivial.) After a Trotter decomposition the exponential of V_I is written in the antinormal representation, but the antinormal symbol (called the 'Glauber function' in Marchioro and Beck (1992)) is only calculated to *first* order in the time increment. In contrast, we suggest using a *higher*-order approximation of that quantity in order to achieve higher accuracy. The results (to be presented in section 5 below) show that a higher-order expansion is indeed very worthwhile: whereas in the application of Marchioro and Beck (1992) (particle in a potential with cubic anharmonicity) the errors become prohibitively large after about two harmonic oscillation periods, we have achieved numerically stable and accurate propagation over up to several thousand periods.

One important difference between this paper and Marchioro and Beck (1992) must be pointed out, however. We employ a 'deterministic' numerical evaluation scheme (to be explained momentarily), whereas Marchioro and Beck employ MC techniques. We would like to stress that our approach could also be combined with MC techniques: as pointed out above, the quantities which have to be evaluated are similar to those in Marchioro and Beck (1992), apart from a higher-order expansion. See also section 6 for some further comments on MC methods.

4. Numerical path integration

For nontrivial Hamiltonians the integrations in equations (14) and (15) have to be performed numerically. Using a quadrature formula

$$\int \frac{\mathrm{d}^2\alpha}{\pi} f(\alpha) \approx \sum_j w_j f(\alpha_j) \tag{17}$$

with fixed sets of abscissas α_j and weights $w_j > 0$, and defining a matrix $P(t/N)$ and a vector v by their elements (here the NCSPI)

$$P_{ij} := \sqrt{w_i w_j}\,\mathrm{e}^{-\mathrm{i}\frac{\omega t}{2N}} \langle \alpha_i \mathrm{e}^{+\mathrm{i}\frac{\omega t}{N}} | \alpha_j \rangle \left(\exp\left(-\frac{\mathrm{i}t}{\hbar N}\tilde{V} \right) \right)_+ (\alpha_i \mathrm{e}^{+\mathrm{i}\frac{\omega t}{2N}}, \alpha_j\, \mathrm{e}^{-\mathrm{i}\frac{\omega t}{2N}}) \tag{18}$$

and

$$v_j := \sqrt{w_j}\langle \alpha_j | \psi \rangle \tag{19}$$

the discretized version of a single time step propagation becomes a matrix–vector multiplication

$$v_i' := \sqrt{w_i}\langle\alpha_i|\mathrm{e}^{-\frac{\mathrm{i}t}{\hbar N}H}|\psi\rangle \simeq \sum_j P_{ij}(t/N)v_j. \tag{20}$$

The vector v' represents the wavepacket propagated by the time t/N. The corresponding matrix $P(t/N)$ for the ACSPI is straightforward:

$$P_{ij} = \sqrt{w_i w_j}\mathrm{e}^{-\mathrm{i}\frac{\omega t}{2N}}\langle\alpha_i \mathrm{e}^{+\mathrm{i}\frac{\omega t}{N}}|\alpha_j\rangle \left(\exp\left(-\frac{\mathrm{i}t}{\hbar N}\tilde{V}\right)\right)_- (\alpha_i \mathrm{e}^{+\mathrm{i}\frac{\omega t}{2N}}) \tag{21}$$

and equation (20) remains the same.

By squaring the matrix $P(t/N)$ one gets a new propagator $P^2(t/N)$ with a doubled time step $2t/N$ (which is a better approximation to the true propagator than $P(2t/N)$). By iteratively squaring the matrix n times, one gets a propagator with an effective time step $\Delta t' = 2^n t/N$ which may be quite long (see the examples in the next section). If N_p denotes the number of points in the grid, a single propagation step requires $\mathcal{O}(N_p^2)$ operations, whereas squaring a matrix is a much more costly $\mathcal{O}(N_p^3)$ step. On the other hand, this single $\mathcal{O}(N_p^3)$ step cuts the total number of necessary $\mathcal{O}(N_p^2)$ steps in half. Obviously this procedure becomes favourable if the states at intermediate times are not of interest and if the total overall propagation time is very long. (This may be due to either very long intrinsic time scales in the problem or to the necessity to propagate many different initial states in a statistical simulation (Saalfrank 1996).) However, in squaring the propagator matrix repeatedly, some care has to be applied in order to avoid numerical instabilities due to accumulation of roundoff errors. In our calculations, we have set matrix elements equal to zero if $|\langle\alpha_i \mathrm{e}^{\mathrm{i}\frac{\omega t}{N}}|\alpha_j\rangle|^2 < \epsilon$, and we have also set vector elements equal to zero after every propagation step if $|v_i|^2 < \epsilon$; we have used $\epsilon = 10^{-12}$. Of course, the appearance of 'explicit zeros' can be used to reduce the number of operations which actually have to be performed in the next matrix multiplication or propagation step, which typically reduces the number of multiplications by 20–30%.

Before one can start with matrix–vector multiplication one has to choose a suitable quadrature formula (17). We treat the real and imaginary parts of the integral separately by one-dimensional, equidistant, symmetric quadrature formulae:

$$\int \mathrm{d}x\, f(x) \simeq \sum_{j=0}^{2M} \Delta f(x_j) \tag{22}$$

with $x_j = (j - M)\,\Delta$. The complex quadrature becomes

$$\int \frac{\mathrm{d}^2\alpha}{\pi} f(\alpha) \simeq \frac{1}{\pi}\sum_{r=0}^{2M}\Delta\sum_{s=0}^{2M}\Delta f(x_r + \mathrm{i}x_s) \tag{23}$$

which can be put into the form of equation (17) by renumbering

$$\alpha_{r+(2M+1)s} = x_r + \mathrm{i}x_s \qquad r, s = 0, \ldots, 2M \tag{24}$$

and $w_j = \Delta^2/\pi$; the number of grid points is thus $N_p = (2M+1)^2$.

We have fixed the mesh size Δ according to the following observation. The scalar product $\langle\alpha|\alpha'\rangle = \langle x + \mathrm{i}y|x' + \mathrm{i}y'\rangle$ (6) contains an oscillatory factor $\exp \mathrm{i}(xy' - yx')$ along with Gaussian factors. The real and imaginary parts of successive α variables in the discretized CSPI thus are related by a Fourier-transform-like operation; they exchange their roles in each integration step and consequently should be treated on the same footing. A discretized finite-bandwidth Fourier transform (with kernel $\exp \mathrm{i}xy$) between two variables, each capable of $2M+1$ symmetrically and equidistantly distributed values ($x = \mu\Delta x$, $y = \mu\Delta y$; $-M \leqslant \mu \leqslant M$) implies a consistency relation between the spacings Δx and Δy, namely

$$\pi = x_{\max}\Delta y = M\Delta x\Delta y. \tag{25}$$

In view of the equivalence between x and y discussed above, the natural choice then is

$$\Delta x = \Delta y = \Delta = \sqrt{\frac{\pi}{M}} \tag{26}$$

increasing M thus means both increasing ($\sim M$) the size of the total area covered by the grid and decreasing ($\sim M^{-1}$) the area of each mesh†.

Before considering some examples it is useful to look at our quadrature formula from another point of view. Since John von Neumann's times (Perelomov 1986) it has been known that any set of coherent states $\{|\alpha_j\rangle\}$ with α_j on an infinite square grid on the complex α-plane with a mesh size $\Delta \leqslant \sqrt{\pi}$ is overcomplete, that means a resolution of unity is possible though not necessarily in the form $\Delta^2/\pi \sum_j |\alpha_j\rangle\langle\alpha_j|$. Recently Zak (1996) pointed out in an analytical study that for a decreasing mesh size $\Delta^2/\pi \sum_j |\alpha_j\rangle\langle\alpha_j|$ approaches the unit operator. Considering this, our quadrature formula also derives directly from a discrete set of coherent states.

5. Numerical examples

In this section we present some numerical examples to demonstrate how the matrix multiplication method (section 4) together with the split-operator method works. Our examples are a double-well potential

$$V(Q) = g\frac{m^2\omega^3}{\hbar}\left(Q - x_0\sqrt{\frac{\hbar}{m\omega}}\right)^2\left(Q + x_0\sqrt{\frac{\hbar}{m\omega}}\right)^2 \tag{27}$$

and the Morse oscillator

$$V(Q) = A\hbar\omega(1 - \mathrm{e}^{-\lambda\sqrt{m\omega/\hbar}Q})^2 \tag{28}$$

where g, x_0, A and λ are dimensionless parameters. While the former is of interest due to the small energy splitting of the two lowest eigenstates, the latter is often used as a model potential for the vibrations of molecules (Braun *et al* 1996). The minima of the double-well potential are situated at the positions $\pm x_0\sqrt{\hbar/m\omega}$, the minimum value of the potential energy is zero, and the frequency of small classical oscillations about the minima is $\Omega = 2x_0\sqrt{2g}\omega$ where ω is the natural frequency of the harmonic oscillator used to define the coherent states. The minimum of the Morse potential is located at zero position and energy, and the small oscillation frequency is $\Omega = \lambda\sqrt{2A}\omega$. By rescaling it is always possible to choose the parameter values such that $\Omega = \omega$ (cf the comment after equation (4)).

In all examples discussed below we use coherent states as initial states $|\psi(t=0)\rangle = |\alpha\rangle$ for some $\alpha \in \mathbb{C}$; of course, more general states can be represented as linear combinations of coherent states, thus our choice means no restriction of generality. (In fact, an initially coherent state quickly ceases to be coherent under the influence of an anharmonic potential.)

As a simple test for our method we calculated the autocorrelation function $\langle\psi(0)|\psi(t)\rangle$ which possesses the spectral representation

$$\langle\psi(0)|\psi(t)\rangle = \sum_m |\langle m|\psi(0)\rangle|^2 \mathrm{e}^{-\mathrm{i}E_m t/\hbar} \tag{29}$$

where $|m\rangle$ are the eigenvectors of the Hamiltonian. The energy eigenvalues can be obtained from (29) by Fourier transformation, with a spectral resolution inversely proportional to the total propagation time. We also calculated the expectation values for position $\langle x\rangle(t)$ and momentum

† We also used a Gauss–Hermite quadrature formula, but we could not see any significant difference to the equidistant quadrature results.

$\langle p\rangle(t)$ and their variances ($\Delta^2 x = \langle x^2\rangle - \langle x\rangle^2$ and $\Delta^2 p = \langle p^2\rangle - \langle p\rangle^2$, respectively) as functions of time. The expectation values $\langle x\rangle$ and $\langle p\rangle$ can be calculated from the expectation value of the annihilation operator $\langle a\rangle$

$$\langle x\rangle(t) = \sqrt{\frac{2\hbar}{m\omega}}\,\mathrm{Re}\langle a\rangle(t) \tag{30}$$

$$\langle p\rangle(t) = \sqrt{2\hbar m\omega}\,\mathrm{Im}\langle a\rangle(t). \tag{31}$$

Similarly $\langle x^2\rangle$ and $\langle p^2\rangle$ follow by antinormal ordering

$$\langle\psi(t)|x^2|\psi(t)\rangle = \frac{\hbar}{m\omega}\int\frac{\mathrm{d}^2\alpha}{\pi}\langle\psi(t)|\alpha\rangle\langle\alpha|\psi(t)\rangle\left(2\,\mathrm{Re}^2\,\alpha - \frac{1}{2}\right) \tag{32}$$

$$\langle\psi(t)|p^2|\psi(t)\rangle = \hbar m\omega\int\frac{\mathrm{d}^2\alpha}{\pi}\langle\psi(t)|\alpha\rangle\langle\alpha|\psi(t)\rangle\left(2\,\mathrm{Im}^2\,\alpha - \frac{1}{2}\right). \tag{33}$$

As unit of time we choose $1/\omega$, so the oscillator period is $T = 2\pi$. Distances are measured in units of $\sqrt{\frac{2\hbar}{m\omega}}$, momenta in units of $\sqrt{2\hbar m\omega}$.

5.1. Double-well potential

In order to give an impression of the most important quantity involved, namely the propagator matrix element $\langle\alpha|\exp(-\mathrm{i}tH/\hbar)|\alpha'\rangle$, we show that quantity as a function of α in figure 1 for fixed $\alpha' = 1.71$ and $t = 4\pi$, for the double-well potential (27). The height coordinate is the modulus of the matrix element. We have visualized the phase in the underlying grey scale; the darkest grey corresponds to phase $\pm\pi$, white signifies phase 0. The double-well nature of the potential is clearly represented by a dominant maximum on the right and a shoulder on the left. Outside the classically accessible region of phase space the propagator decays rapidly. It is important to note that the phase of the propagator varies only very slowly in the region where its magnitude is appreciable and still not very rapidly in the outer regions where the magnitude is small anyway. In comparison, real-space propagators are notorious for being much less well behaved. The free-particle propagator, for instance, is proportional to $\exp(\mathrm{i}m(x-x')^2/2\hbar t)$ and thus oscillates progressively faster as $x - x'$ grows. The taming of these oscillations by sophisticated mathematical approximation techniques has involved a large amount of work by several groups†. The coherent-state propagator, in contrast, is smooth by nature.

At this point we would like to point out an additional benefit of the coherent-state representation. For an arbitrary pure quantum state $|\psi\rangle$, the Husimi density (Takahashi 1989, Cahill and Glauber 1969) $\rho(\alpha) := |\langle\psi|\alpha\rangle|^2$ is a phase space density which yields insight into the quantum dynamics in the classical framework of phase space. The Husimi density shows precisely the amount of phase space structure allowed by the uncertainty relation, in contrast to the popular Wigner distribution (Cahill and Glauber 1969, Wigner 1932, Louisell 1973) which displays violent oscillations between positive and negative values on phase space scales smaller than the uncertainty limit. (In fact, the Husimi density can be obtained from the Wigner function by a Gaussian smoothing (Cartwright 1976) procedure.) The modulus-squared of the quantity shown in figure 1 is the Husimi density of the state resulting from the initial $|\alpha'\rangle$ after $t = 4\pi$. Thus propagation via coherent states yields at any intermediate time the valuable phase space information contained in the Husimi density‡.

We now discuss some examples of initially coherent states propagated in the double-well potential. Because of the symmetry of the double-well potential, all eigenfunctions are either

† Makri (1995) and references cited therein; Mak and Egger (1996), and other contributions therein.

‡ In fact, the formulae (30)–(33) can be viewed as averages of phase space functions with respect to the Husimi density.

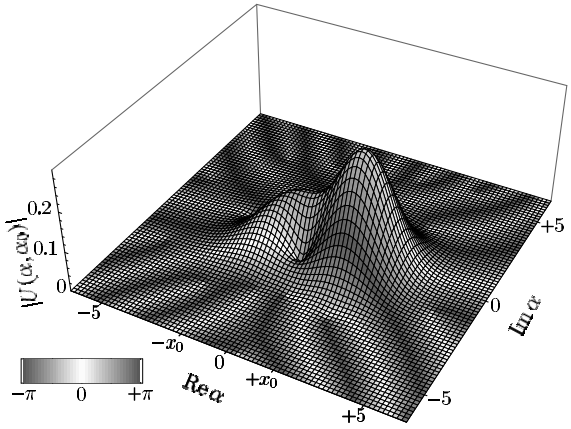

Figure 1. Double-well potential $V(x) = g(x^2 - x_0^2)^2$ with $g = \frac{1}{50}$ and $x_0 = \frac{5}{2}$ (energies are measured in units of $\hbar\omega$, lengths in units of $\sqrt{\hbar/m\omega}$). The propagator matrix element $U(\alpha, \alpha') = \langle\alpha|\mathrm{e}^{-\mathrm{i}tH/\hbar}|\alpha'\rangle$ for $\alpha' = 1.71$ and $t = 4\pi$ is shown. The height coordinate is the modulus of the matrix element. We have visualized the phase in the underlying grey scale; the darkest grey corresponds to phase $\pm\pi$, white signifies phase 0. (It should be noted that the grey scale seems to suggest a height variation, in particular away from the centre of the figure; however, a closer look at the grid lines reveals that this is an optical artifact.) The double-well nature of the potential is clearly represented by a dominant maximum on the right and a shoulder on the left. Outside the classically accessible region of phase space the propagator decays rapidly. It is important to note that the phase of the propagator varies only very slowly in the region where its magnitude is appreciable and still not very rapidly in the outer regions where the magnitude is small anyway. Technical data: $M = 13$, NCSPI, $\Delta t = 2\pi/512$, $\Delta t' = 4\Delta t$, fourth-order expansion.

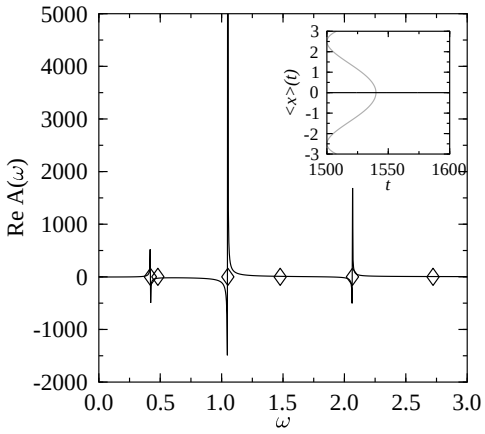

Figure 2. Double-well potential $V(x) = g(x^2 - x_0^2)^2$ with $g = \frac{1}{50}$ and $x_0 = \frac{5}{2}$ (energies are measured in units of $\hbar\omega$, lengths in units of $\sqrt{\hbar/m\omega}$). Main plot: real part Re $A(\omega)$ of the Fourier transform of the autocorrelation function $\langle\psi(0)|\psi(t)\rangle$ with initial state $|\psi(0)\rangle = |\alpha = 0\rangle$. Eigenvalues of the double-well potential are marked by $\diamondsuit$; only eigenvalues belonging to even states appear in the spectrum, because the initial state is even. The total propagation time is $T = 512\pi$, therefore the spectral resolution is $\Delta\omega = \pi/512 \approx 0.0061$. Inset: expectation value $\langle x\rangle$ is—as it should be—constant. Technical data: $M = 13$, NCSPI, $\Delta t = 2\pi/512$, $\Delta t' = 4\Delta t$, fourth-order expansion.

symmetric or antisymmetric. It follows that, if one starts with a symmetric or antisymmetric state, the time propagation preserves this symmetry, because only eigenfunctions of the same symmetry contribute to the state. In figure 2 the spectrum of the autocorrelation function is shown for an initial state $|\psi(t = 0)\rangle = |0\rangle$. This means that the initial state is symmetric. In agreement with the above arguments, only even eigenvalues can be seen in the spectrum. The expectation value $\langle x\rangle$ of the position operator is precisely zero over a very long time (see inset of figure 2), which indicates that our method is stable. Of course this does not mean that the state is stationary; for example its width oscillates quasi-periodically. Figure 3 shows the expectation value $\langle x\rangle(t)$ and the standard deviation $\Delta x := \sqrt{\Delta^2 x}$ for the initial state

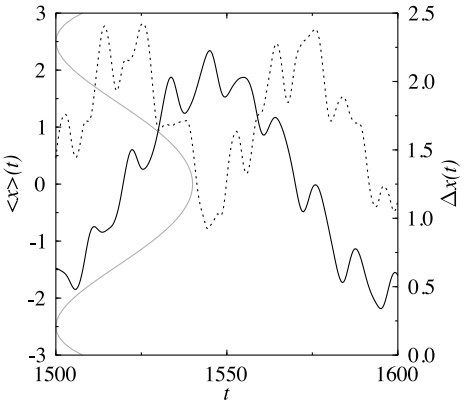

Figure 3. Double-well potential (see figure 2 for parameters). Expectation value of x with initial state $|\psi(0)\rangle = |\alpha = 5/\sqrt{8}\rangle$ (full curve). The tunnelling time is about 50 time units. The uncertainty Δx (dotted curve) is smallest whenever the expectation value $\langle x\rangle$ comes close to one of the minima of the potential, and reaches a maximum whenever $\langle x\rangle$ is 'below the potential barrier'. The potential is also shown schematically. Technical data: $M = 13$, NCSPI, $\Delta t = 2\pi/512$, $\Delta t' = 32\Delta t$, fourth-order expansion.

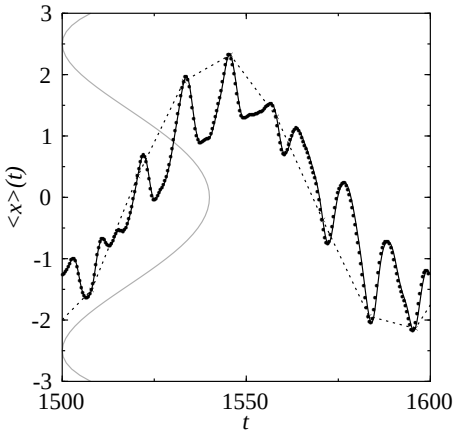

Figure 4. Double-well potential (see figure 2 for parameters). Expectation value of x with initial state $|\psi(0)\rangle = |\alpha = 2\rangle$. Two different effective time steps are used: $\Delta t' = 32\Delta t$ (·), $\Delta t' = 1024\Delta t$ (×); lines connecting the symbols are to guide the eye. Both data sets coincide at equal sampling times, indicating that repeated matrix squaring does not harm the accuracy. The larger effective time step corresponds to two periods of the harmonic oscillation frequency about the potential minima. Technical data: $M = 13$, NCSPI, $\Delta t = 2\pi/512$, fourth-order expansion.

$|\alpha = 5/\sqrt{8}\rangle$ centred at one of the potential minima. The expectation value moves back and forth between the two wells in a characteristic time τ. This is a tunnelling motion, because the total energy $\langle H\rangle = 0.515$ is smaller than the height of the barrier ($V(0) = 0.8$). The localized wavepacket does not tunnel as a compact object, but it rather expands while the expectation value moves to the maximum of the potential and contracts while the expectation value moves to the other minimum. The difference $\Delta\omega = 0.06$ of the two lowest eigenvalues gives the tunnelling time τ for a wavepacket moving from one well to the other:

$$\tau = \frac{\pi}{\Delta\omega} \approx 52.3. \tag{34}$$

A second timescale is given by the energy differences between other low-lying energy levels. This can also be seen in figure 4, where the initial state is $|\alpha = 2\rangle$. Here we used two different kinds of propagator matrices: for both we used an elementary time step $\Delta t = 2\pi/512$, and we squared these propagators five and ten times, therefore the effective time steps are $32\Delta t$ and $1024\Delta t$, respectively. Every 32nd point of the discretized trajectory calculated with the smaller time step coincides with a point calculated with the longer time step, even after a long total propagation time. This shows that repeated matrix multiplication is stable. To demonstrate this more clearly, we propagated an initial state $|\psi\rangle$ by different propagators: As a reference state we propagated $|\psi\rangle$ by the plain propagator $P(t/N)$ to get $|\psi_0(T)\rangle$ after k vector–matrix multiplications (where $T = kt/N$), a second state we get by first squaring the plain propagator ν-times, which means an effective step size $\Delta t' = 2^\nu t/N$ and then doing $k/2^\nu$ vector–matrix multiplications to get a state $|\psi_\nu(T)\rangle$. For demonstrating the consistency of both results, we calculated the overlap $C_\nu(T) = \langle\psi_0(T)|\psi_\nu(T)\rangle$ between the final states obtained by the two procedures. As an elementary time step we took $\Delta t = 2\pi/256$ and propagated the initial state $|\alpha = 2\rangle$ 2^{19} times to get the reference state $|\psi_0(T)\rangle$, therefore $T = 4096\pi$ (approximately 246

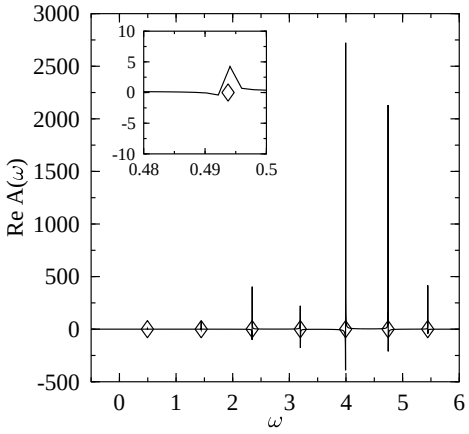

Figure 5. Morse potential $V(x) = A(1 - \exp(-\lambda x))^2$ with $A = 10$ and $\lambda = 1/\sqrt{20}$ (energies are measured in units of $\hbar\omega$, lengths in units of $\sqrt{\hbar/m\omega}$). Main plot: real part Re $A(\omega)$ of the spectrum of the autocorrelation function $\langle\psi(0)|\psi(t)\rangle$ with initial state $|\psi(0)\rangle = |\alpha = 3\rangle$. The total propagation time is $T = 131\,072\pi/125$, therefore the spectral resolution is $\Delta\omega = 125\pi/131\,072 \approx 0.003$. Within this accuracy the peaks coincide with the exact eigenvalues (◇). Inset: shows the lowest peak of the spectrum; its position is $E_0 = \frac{79}{160}$. Technical data: $M = 17$, NCSPI, $\Delta t = 2\pi/2000$, $\Delta t' = 128\Delta t$, tenth-order expansion.

tunnelling periods). For $\nu = 1, 2, 3, \ldots$ the final states $|\psi_\nu(T)\rangle$ were calculated as described above, and the C_ν values are shown in table 1. The norms of the final states differ slightly from unity, but the overlaps $C_\nu(T)$ agree with $\||\psi_\nu(T)\rangle\|^2$ to high precision. That indicates that the propagation over a long time indeed causes a slight loss of probability, but that loss is not related to the effective time step size. We conclude that repeated matrix multiplication does not affect the accuracy, and is therefore stable. This offers the opportunity of working with a rather long time step whenever fine resolution in time is not essential.

Table 1. Double-well potential (see figure 2). The overlaps $C_\nu(T) = \langle\psi_0(T)|\psi_\nu(T)\rangle$ for different ν are shown (for explanations refer to the text). Although the norms (5th column) of all final states deviate significantly from 1, the C_ν do not depend on ν and the real parts of the C_ν are equal to the squares of the norms, showing that the results for different repeatedly squared propagators are consistent with each other. The precision can be improved by using a smaller time step Δt. In the second column the effective time step $\Delta t' = 2^\nu \Delta t$ is given. Technical data: $M = 13$, NCSPI, $\Delta t = 2\pi/256$, fourth-order expansion, total propagation time $T \approx 4096\pi$. The initial state was $|\alpha = 2\rangle$.

ν	$\Delta t'$	Re $C_\nu(T)$	Im $C_\nu(T)$	$\||\psi_\nu(T)\rangle\|$
0	0.024 544 00	0.984 7179	$-3.010\,427 \times 10^{-20}$	0.992 3295
1	0.049 088 00	0.984 7189	$4.786\,793 \times 10^{-8}$	0.992 3306
2	0.098 176 00	0.984 7194	$4.600\,942 \times 10^{-8}$	0.992 3311
3	0.196 352 0	0.984 7196	$4.650\,630 \times 10^{-8}$	0.992 3314
4	0.392 704 0	0.984 7197	$4.633\,073 \times 10^{-8}$	0.992 3315
5	0.785 408 0	0.984 7197	$4.612\,626 \times 10^{-8}$	0.992 3316
6	1.570 816	0.984 7197	$4.633\,432 \times 10^{-8}$	0.992 3316
7	3.141 632	0.984 7197	$4.633\,546 \times 10^{-8}$	0.992 3316
8	6.283 264	0.984 7197	$4.636\,670 \times 10^{-8}$	0.992 3316
10	12.566 53	0.984 7197	$4.636\,517 \times 10^{-8}$	0.992 3316
11	25.133 06	0.984 7197	$4.638\,332 \times 10^{-8}$	0.992 3316
12	50.266 11	0.984 7197	$4.638\,827 \times 10^{-8}$	0.992 3316
13	100.532 2	0.984 7197	$4.640\,010 \times 10^{-8}$	0.992 3316
14	201.064 5	0.984 7197	$4.639\,162 \times 10^{-8}$	0.992 3316
15	402.128 9	0.984 7197	$4.639\,972 \times 10^{-8}$	0.992 3316
16	804.257 8	0.984 7197	$4.640\,011 \times 10^{-8}$	0.992 3316

Table 2. Norm of the state $|\psi(t)\rangle$ was taken after a propagation time $t \approx 1600$ (depending on the multiple of $\Delta t'$) in a Morse potential (see figure 5 for parameters), using the normal ordered coherent-state path integral. Different step sizes Δt and different orders n_0 of the series expansion of the anharmonic time evolution operator were used. The asterisk marks a numerical overflow after a small propagation time (e.g. $t \approx 18$). Technical data: $M = 15$, NCSPI, $|\psi(0)\rangle = |\alpha = 2\rangle$, $\Delta t' = 2^7 \Delta t$.

	Step size Δt		
n_0	$2\pi/1024$	$2\pi/1536$	$2\pi/2048$
3	*	*	0.971 4917
4	*	0.999 3492	0.999 2865
6	*	0.999 3756	0.999 2927
8	*	0.999 3756	0.999 2931
10	*	0.999 3756	0.999 2927

5.2. Morse potential

As a second example we consider the Morse potential (equation (28)), which has been widely used as a model for the vibrations of molecules (Braun *et al* 1996). The Morse potential (Landau and Lifshitz 1958) has only a finite number of bound states with energy eigenvalues

$$E_\nu = -A\hbar\omega \left\{ \left[1 - \frac{\lambda}{\sqrt{2A}} \left(\nu + \frac{1}{2} \right) \right]^2 - 1 \right\} \qquad \text{where} \quad 0 \leqslant \nu < \frac{\sqrt{2A}}{\lambda} - \frac{1}{2}. \tag{35}$$

To demonstrate the practical value of our method, we chose the parameters such that the potential has only a few bound states: $A = 10$, $\lambda = 1/\sqrt{2A} = 1/\sqrt{20}$, therefore we have 20 discrete eigenvalues. This choice of parameters means that the potential is strongly anharmonic, and we are far from treating the harmonic oscillator. This can be seen in figure 5, where we show the spectrum obtained from long-time propagation of an initial state $|\alpha = 3\rangle$. The deviation from the harmonic spectrum $E_\nu/\hbar\omega = \frac{1}{2}, \frac{3}{2}, \frac{5}{2}, \ldots$ compared with $E_\nu/\hbar\omega = \frac{79}{160}, \frac{231}{160}, \frac{75}{32}, \frac{511}{160}, \frac{639}{160}, \ldots$ is obvious, while the agreement with the exact values is as good as the precision of the spectrum. Also worth mentioning is the revival (Averbukh and Perelman 1989, Meier and Engel 1995) of the initial state after a revival time $T_{\text{rev}} \approx 125.66$, visible in figure 6, where the autocorrelation climbs up to almost the maximum value of unity after T_{rev}. This revival time is due to the fact that the initial state $|\psi_0\rangle = |\alpha = 3\rangle$ can be approximated by a superposition of the eigenstates $|\nu = 3\rangle$, $|\nu = 4\rangle$, and $|\nu = 5\rangle$:

$$|\psi(t)\rangle \approx \sum_{\nu=3}^{5} a_\nu \mathrm{e}^{-\mathrm{i}E_\nu t} |\nu\rangle. \tag{36}$$

Considering this, the autocorrelation function is given to a good approximation by

$$\langle\psi(0)|\psi(t)\rangle \approx \mathrm{e}^{-\mathrm{i}E_3 t}(|a_3|^2 + |a_4|^4 \mathrm{e}^{-\mathrm{i}(E_4 - E_3)t} + |a_5|^2 \mathrm{e}^{-\mathrm{i}(E_5 - E_3)t}). \tag{37}$$

As one can immediately see, the modulus of this correlation function reaches its maximum value at times t, when both $(E_4 - E_3)t/2\pi$ and $(E_5 - E_3)t/2\pi$ are integers; therefore the revival time is $T_{\text{rev}} = 40\pi \approx 125.66$.

To demonstrate the dependence of the precision on the grid size, we propagated an initial state with different grid sizes, and traced the norm of the state. From figure 7, it can be seen that the smaller the grid is the faster the norm decays. This behaviour is as one expects *a priori*, because if the grid does not cover the physically relevant part of the α-plane, important contributions to the wavepacket will get lost. Another point to mention is the dependence of accuracy on the type of path integral used, either normal- or antinormal-ordered. In tables 2

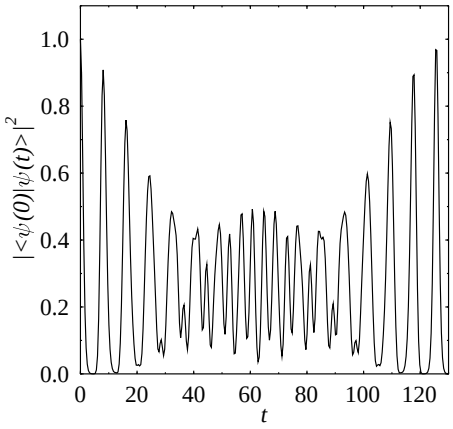

Figure 6. Morse potential (see figure 5 for parameters). Modulus of the autocorrelation function $\langle\psi(0)|\psi(t)\rangle$ with initial state $|\psi(0)\rangle = |\alpha = 3\rangle$. After a time $T_{\text{rev}} \approx 125$ the system almost returns to its initial state; this behaviour is called a revival. Technical data: $M = 17$, NCSPI, $\Delta t = 2\pi/2000$, $\Delta t' = 128\Delta t$, tenth-order expansion.

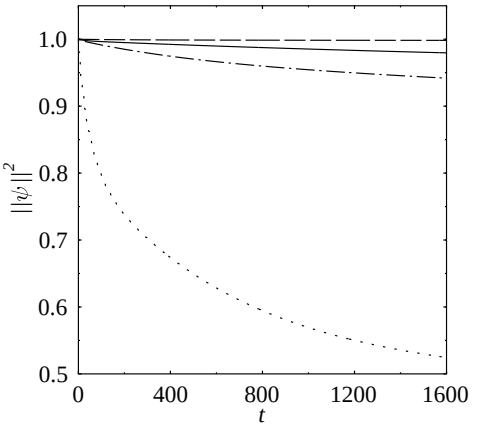

Figure 7. Morse potential (see figure 5 for parameters). Norms of the propagated states $|\psi(0)\rangle = |\alpha = 3\rangle$ and $|\psi(0)\rangle = |\alpha = 2\rangle$ for different grid sizes. For the initial state $|\psi(0)\rangle = |\alpha = 3\rangle$ even the largest grid size ($M = 15$, full curve) leads to a significant leakage of the norm, while for the state $|\psi(0)\rangle = |\alpha = 2\rangle$, starting well inside the integration area, even a grid size of $M = 13$ (broken curve) is better than the above one. Dotted curve: $|\psi(0)\rangle = |\alpha = 3\rangle$, $M = 9$. Dot-dashed curve: $|\psi(0)\rangle = |\alpha = 2\rangle$, $M = 9$. Technical data: NCSPI, $\Delta t = 2\pi/2048$, $\Delta t' = 256\Delta t$, tenth-order expansion.

Table 3. The same as table 2, but for antinormal ordered coherent-state path integral. Higher order allows the use of bigger time steps, while smaller time steps do not guarantee higher accuracy. Technical data: $M = 15$, ACSPI, $|\psi(0)\rangle = |\alpha = 2\rangle$, $\Delta t' = 2^7\Delta t$.

	Step size Δt			
n_0	$2\pi/790$	$2\pi/800$	$2\pi/1024$	$2\pi/2048$
3	*	*	*	0.971 4917
4	*	*	0.999 3114	0.999 3010
6	*	0.999 5818	0.999 5128	0.999 3072
8	0.999 5850	0.999 5816	0.999 5128	0.999 3072
10	0.999 5850	0.999 5864	0.999 5128	0.999 3072

and 3 we show the norm of the propagated state after a total propagation time of 1600 time units. We used different elementary time steps Δt, different orders for the propagator and both kinds of symbols. As one can see from the results for normal-ordered symbol, a big time step Δt gives numerical non-sense; in fact, a numerical overflow appears after only a few propagation steps. On the other hand a smaller time step does not guarantee a higher accuracy, because a smaller time step means more multiplications to reach the same total propagation time, increasing the influence of numerical noise. But as one also can see from table 3, a higher order in the series expansion of the symbol of $\exp(-\frac{\mathrm{i}}{\hbar}\Delta t\tilde{V})$ permits a bigger time step Δt; in fact, order eight gives about the accuracy as does order four, with a time step half as big.

In comparison with configuration space techniques, we need fewer grid points†. This might be understood from the fact that coherent states already bear the right amount of quantum fluctuations, whereas configuration space methods have to mimic these fluctuations by sampling over many δ-functions (or plane waves).

6. Conclusions

We presented a first systematic study of the numerical applicability of coherent-state path integrals to one-dimensional (standard) Hamiltonians in quantum dynamics. For doing CSPI an approximation of the propagator in terms of (anti-)normal symbols is required; we chose a Taylor expansion‡ of the exponential. That requires the (anti-)normal ordering of powers of the Hamiltonian which we reduced further to the (anti-)normal ordering of the potential only by the split-operator technique. The wavepacket is represented on a grid of points in the complex plane, and the time propagation of the wavefunction is done by a vector–matrix multiplication. We have achieved stable propagation over very long times, and we have shown that one can get an effective matrix propagator with an effective time step much larger than the elementary time step by repeated matrix multiplication without losing accuracy. We have also applied our method to time-dependent problems, for example to the motion of a particle in a sinusoidally driven double well (Burghardt and Stolze 1999). For a particular combination of driving amplitude and frequency the tunnelling motion of the particle can be dynamically suppressed (Grossman *et al* 1991). The observation of this 'coherent destruction of tunnelling' requires stable propagation of the initial state over time intervals still longer than those considered here.

We have restricted our study to bound motion in simple well-type potentials. We wish to stress that this is not a principal restriction. An initially localized wavepacket may be followed for some limited time even in a non-confining potential, until it eventually leaves (partially or completely) the finite grid used in a numerical calculation. This is true for both coordinate-space and phase space methods. However, genuine scattering problems involving final wavepackets at infinity should be treated by more appropriated methods.

The matrix multiplication (MM) approach discussed in this paper is limited to low-dimensional systems, because the size of the matrices involved grows exponentially with the dimension. It is therefore interesting to discuss MC evaluation of CSPI as an alternative, potentially less dimension-limited scheme. The split-operator approximation for the short-time propagator developed in section 3 may be incorporated in a MC path integration scheme. This was demonstrated by Marchioro and Beck (1992) for a similar (but less accurate) propagator. The main limitation of the MC approach concerns the size of the time step. In the MM approach, one may construct an effective propagator matrix corresponding to a very long effective time step, as discussed in section 4 and demonstrated in section 5. This is not possible in the MC approach, where one is forced to stick to the elementary time step restricted by the precision of the elementary propagator§. In contrast to MM, the MC approach in higher dimensions is not impeded by a rapidly growing demand for computer memory. However, in order to obtain data with a prescribed statistical precision, a rapidly growing number of paths have to be sampled as the dimension (or the total propagation time) grows. Thus, employing MC instead of MM methods means trading cpu time for memory, a situation quite familiar for major computer

† For example, we used 729 grid points in the α-plane ($M = 13$) for the Morse potential with the same parameter values as in Braun *et al* (1996), while the authors of that reference used 2048 grid points on the real x-line.

‡ Alternative options well worth studying would include cumulant expansions or expansions in a Chebyshev series, both of which have in fact been employed in other wavepacket propagation algorithms.

§ If the dimension is not too high, however, one might think of 'hybrid' methods evaluating (by MC) sums over paths on a fixed lattice of phase space points, with an effective propagator matrix calculated once and for all by MM.

applications in science. Finally, we want to remark that, even though MM methods, in contrast to MC methods, are restricted to low-dimensional systems, there are still many interesting low-dimensional problems being investigated by non-MC propagation methods (Saalfrank 1996, Grossman *et al* 1991).

We have demonstrated that numerical evaluation of CSPI can be significantly improved as compared with the pioneering studies (Marchioro 1990, Marchioro and Beck 1992), and we believe that application of some of the ideas which were successfully used for configuration space path integrals (smoothing techniques based on stationary-phase ideas, Fourier coefficient path integration etc) holds the potential for further significant improvement of CSPI as a numerical tool.

Modern configuration-space-based wavepacket propagation methods often employ fast Fourier transforms to switch between coordinate and momentum representations. This makes these methods more efficient than matrix multiplication methods based on the coordinate grid. However, our method needs fewer grid points for the discretized wavefunction, and therefore it will be interesting to find out if our method (or future refinements of it) can compete with other propagation methods in practice.

Acknowledgment

This work was supported by the Deutsche Forschungsgemeinschaft through the Schwerpunktprogramm: Zeitabhängige Phänomene und Methoden in Quantensystemen der Physik und Chemie.

References

Adachi S 1989 *Ann. Phys.* **195** 45–93
Averbukh I S and Perelman N F 1989 *Sov. Phys.–JETP* **69** 464–9
Braun M, Meier C and Engel V 1996 *Comput. Phys. Commun.* **93** 152–8
Burghardt B, Eicke J and Stolze J 1998 *J. Chem. Phys.* **108** 1562–9
Burghardt B and Stolze J 1999 *Path-Integrals from peV to TeV—50 Years from Feynman's Paper* (Florence: World Scientific) to be published
Cahill K E and Glauber R L 1969 *Phys. Rev.* **177** 1857–81
Caratzoulas S and Pechukas P 1996 *J. Phys. Chem.* **104** 6265–77
Cartwright N D 1976 *Physica* A **83** 210–12
Feit M D, Fleck J A Fr and Steiger A 1982 *J. Comput. Phys.* **47** 412–33
Grossmann F, Dittrich T, Jung P and Hänggi P 1991 *Phys. Rev. Lett.* **67** 516–19
Klauder J R and Skagerstam B 1985 *Coherent States* (Singapore: World Scientific)
Kosloff R 1994 *Annu. Rev. Phys. Chem.* **45** 145–78
Landau L D and Lifshitz E M 1958 *Quantum Mechanics* (London: Pergamon)
Leforestier C *et al* 1991 *J. Comput. Phys.* **94** 59–80
Leschke H 1979 *Feynman Path Integrals (Lecture Notes in Physics vol 106)* (Berlin: Springer) p 435
Louisell W H 1973 *Quantum Statistical Properties of Radiation* (New York: Wiley)
Mak C H and Andersen H C 1990 *J. Chem. Phys.* **92** 2953–65
Mak C H and Egger R 1996 *New Methods in Computational Quantum Mechanics (Adv. Chem. Phys. XCIII)* ed I Prigogine and S Rice (New York: Wiley) pp 39–76
Makri N 1995 *J. Math. Phys.* **36** 2430–57
Marchioro II T L 1990 *J. Math. Phys.* **31** 2935–45
Marchioro II T L and Beck T 1992 *J. Chem. Phys.* **96** 2966–77
Meier C and Engel V 1995 *Femtosecond Chemistry* vol 1, ed J Manz and L Wöste (Weinheim: VCH Verlagsgesellschaft) ch 11, pp 369–94
Perelomov A 1986 *Generalized Coherent States and Their Applications* (Berlin: Springer)
Prates Ramalho J P, Costa Cabral B J and Silva Fernandes F M S 1993 *J. Phys. Chem.* **98** 3300–5
Saalfrank P 1996 *Chem. Phys.* **211** 265–76

Schulman L S 1981 *Techniques and Applications of Path Integration* (New York: Wiley)
Storer R G 1968 *J. Math. Phys.* **9** 964–70
Takahashi K 1989 *Prog. Theor. Phys. Suppl.* **98** 109–56
Wigner E P 1932 *Phys. Rev.* **40** 749–59
Zak J 1996 *J. Math. Phys.* **37** 3815–23